https://doi.org/10.1016/j.envpol.2020.116285

Long-term variations of C_1-C_5 alkyl nitrates and their sources in Hong Kong

Lewei Zeng[1], Hai Guo[1*], Xiaopu Lyu[1], Beining Zhou[1], Zhenhao Ling[2], Isobel J. Simpson[3], Simone Meinardi[3], Barbara Barletta[3], Donald R. Blake[3]

[1]Air Quality Studies, Department of Civil and Environmental Engineering, The Hong Kong Polytechnic University, Hong Kong, China

[2]School of Atmospheric Sciences, Sun Yat-sen University, Guangzhou, China

[3]Department of Chemistry, University of California at Irvine, USA

*Corresponding author. ceguohai@polyu.edu.hk

Abstract

Investigating the long-term trends of alkyl nitrates ($RONO_2$) is of great importance for evaluating the variations of photochemical pollution. Mixing ratios of C_1-C_5 $RONO_2$ were measured in autumn Hong Kong from 2002 to 2016, and the average level of 2-butyl nitrate (2-$BuONO_2$) always ranked first. The C_1-C_4 $RONO_2$ all showed increasing trends ($p < 0.05$), and 2-$BuONO_2$ had the largest increase rate. The enhancement in C_3 $RONO_2$ was partially related to elevated propane, and dramatic decreases ($p < 0.05$) in both nitrogen monoxide (NO) and nitrogen dioxide (NO_2) also led to the increased $RONO_2$ formation. In addition, an increase of hydroxyl (OH) and hydroperoxyl (HO_2) radicals ($p < 0.05$) suggested enhanced atmospheric oxidative capacity, further resulting in the increases of $RONO_2$. Source apportionment of C_1-C_4 $RONO_2$ specified three typical sources of $RONO_2$, including biomass burning emission, oceanic emission, and secondary formation, of which secondary formation was the largest contributor to ambient $RONO_2$ levels. Mixing ratios of total $RONO_2$ from each source were quantified and their temporal variations were investigated. Elevated $RONO_2$ from secondary formation and biomass burning emission were two likely causes of increased ambient $RONO_2$. By looking into the spatial distributions of C_1-C_5 $RONO_2$, regional transport from the Pearl River Delta (PRD) was inferred to build up $RONO_2$ levels in Hong Kong, especially in the northwestern part. In addition, more serious $RONO_2$ pollution was found in western PRD region. This study helps build a comprehensive understanding of $RONO_2$ pollution in Hong Kong and even the entire PRD.

Key words: $RONO_2$; Long-term trend; Source apportionment; Hong Kong

Capsule: Elevated secondary formation and biomass burning emission caused $RONO_2$ increase from 2002 to 2016.

1 Introduction

Alkyl nitrates ($RONO_2$), as typical components of organic nitrates in the atmosphere, are mainly formed through the reactions between volatile organic compounds (VOCs) and nitrogen oxides ($NO_x = NO + NO_2$) in the presence of sunlight, similar to ozone (O_3) production. Due to their relatively long lifetimes (days to months), $RONO_2$ can travel long distances and contribute to free radicals and NO_x levels in remote areas, acting as temporary reservoirs of reactive nitrogen (Clemitshaw et al., 1997), hence affecting regional and global air quality.

Previous observations of gaseous C_1-C_5 $RONO_2$ (full names and abbreviations are listed in Table S1 for reference) reported that mixing ratios of individual $RONO_2$ ranged from tens to hundreds of pptv (part per trillion by volume), and 2-$BuONO_2$ was always the most abundant in air masses with continental characteristics (Barletta et al., 2002; Simpson et al., 2003, 2006). Ambient $RONO_2$ are mostly derived from photochemical formation, as branching reactions in the process of O_3 formation (Atkinson et al., 1990; Carter et al., 1989; Lyu et al., 2017a). VOCs and NO_x are recognized as important precursors in $RONO_2$ formation (Atkinson et al., 1982; Carter et al., 1989). Early research (Atkinson et al., 1982; Bertman et al., 1995) emphasized the prominent roles of parent hydrocarbons (HCs), especially for those with larger carbon numbers, *i.e.*, C_4-C_5 $RONO_2$. Later, the importance of VOCs other than parent hydrocarbons was demonstrated, especially for C_1-C_3 $RONO_2$ formation (Flocke et al., 1998; Sommariva et al., 2008; Worton et al., 2010). Contributions of different groups of VOCs to $RONO_2$ production were quantified in both NO_x-rich and NO_x-lean environments (Zeng et al., 2018). The impact of VOC precursors includes direct decomposition to C_1-C_5 peroxy and alkoxy radicals (RO_2/RO) as well as regulation of atmospheric oxidative capacity, which influences formation efficiency of $RONO_2$ (Lyu et al., 2017a; Zeng et al., 2018).

Apart from photochemical formation, primary emissions are ambient $RONO_2$ sources. Atlas et al. (1993) and Chuck et al. (2002) both reported the emissions of $RONO_2$ from the oceans, especially for C_1-C_2 $RONO_2$. Biomass burning was revealed as another $RONO_2$ source (Simpson et al., 2002; Blake et al., 2003; Lyu et al., 2017a).

Temporal variations of $RONO_2$ have been widely studied, and most studies focused on seasonal variations. Aircraft campaigns of $RONO_2$ over the Pacific Ocean date back to the last century (Fisher et al., 2018), in which winter peaks and summer troughs were observed (Blake et al., 2003). A similar phenomenon was captured in Greenland (Swanson et al., 2003). However, in urban/suburban areas, $RONO_2$ peaked under the influence of polluted air masses (Day et al., 2003). For example, in Hong Kong $RONO_2$ reached a peak in autumn when northerly winds dominated, bringing in pollutants from mainland China (Simpson et al., 2006).

Being the most developed and populated city in South China, Hong Kong has suffered from severe photochemical pollution in the past decades, with increased ambient O_3 levels (Wang et al., 2009; Wang et al., 2017a). As important indicators of photochemical pollution, long-term variations of $RONO_2$ are worth investigating to evaluate the variations of secondary pollution, to better understand atmospheric chemistry, and to help refine control strategies from a long-term perspective. Up to now, very limited research on the yearly variations of $RONO_2$ has been undertaken around the world except for aircraft observations over remote marine areas (Fisher et al., 2018), which leaves a gap in long-term $RONO_2$ pollution under the influence of continental air masses. We for the first time investigated the temporal patterns of $RONO_2$ levels and their sources in Hong Kong, South China.

In this study, observational data from 2002 to 2016 in Hong Kong were analyzed to obtain the long-term trends of $RONO_2$ and their precursors. Variation of atmospheric reactivity during the study period was also characterized. In addition, source apportionment of $RONO_2$ was conducted to quantify the contributions of both primary and secondary sources. This study helps to build a comprehensive understanding of $RONO_2$ pollution in Hong Kong in the past 15 years.

2 Methodology

2.1 Data source

In this study, five intensive field measurements were conducted in Hong Kong in 2002, 2006, 2010, 2013 and 2016. Figure S1 shows the geographical locations of the sampling sites (Tung Chung site (TC), 22.28°N, 113.94°E; Tsuen Wan site (TW), 22.37°N, 114.11°E) in Hong Kong. The TC site is located in an emerging town in southwestern Hong Kong, adjacent to the Pearl River Estuary (PRE), ~3 km southeast of Hong Kong International Airport and ~20 km southwest of Hong Kong. It is surrounded by commercial and residential areas. The sampling site was set up on the rooftop of a six-story building (~20 m above ground level (a.g.l.)). It has been recognized that air pollution at TC is attributable to both local emissions and regional transport (Wang et al., 2005; Guo et al., 2006; Xue et al., 2014). For example, an increase of O_3 was often observed in autumn, when dominant northerly winds brought in polluted continental air masses from the Pearl River Delta (PRD) region in mainland China to Hong Kong and weather conditions were favorable for secondary pollutant formation (Wang et al., 2009; Wang et al., 2017b). The TW site (~17 m a.g.l.) is located in western Hong Kong, ~20 km northeast of TC site. It is surrounded by newly developed zones mainly engaged in residential and commercial activities, and its land use functions are similar to the TC site.

All samples (except 2010) were collected at TC while samples in 2010 were obtained at TW. Given the fact that the lifetime of C_1-C_5 $RONO_2$ usually ranges from days to months (Clemitshaw et al., 1997), the spatial variations of $RONO_2$ between these two sites are expected to be minor (C_5 $RONO_2$ were measured beginning in 2013). The uncertainty of long-term variations caused by different sampling sites was considered in the following data analysis (section 3.2). In addition, since $RONO_2$ levels are relatively higher in autumn in Hong Kong than in other months (Simpson et al., 2006) due to more intensive photochemistry and/or more regional transport from mainland China (Wang et al., 2017a; Zeng et al., 2018), here we only selected samples collected in autumn (September, October and November) for further analysis in order to eliminate seasonal influences and better reflect the photochemistry in Hong Kong.

In addition, a grid study was carried out in autumn of 2014 to study the spatial patterns of $RONO_2$ in Hong Kong (geographical locations marked as gray dots in Figure S1 and described in Table S2). In addition, $RONO_2$ observation data from ten sampling sites in nine cities (*i.e.*, Guangzhou (two sampling sites), Shenzhen, Zhuhai, Foshan, Zhaoqing, Jiangmen, Huizhou, Dongguan, Zhongshan) in inland PRD were collected in winter and summer of 2018 (geographical locations as shown in Figure S1) to study the spatial distributions of $RONO_2$ in the PRD region. The ten sampling sites were all situated in urban/suburban areas to better represent spatial distributions of $RONO_2$ in this region.

During all sampling campaigns, whole air samples were collected offline in the daytime (7:00-19:00) using 2-L single port stainless steel canisters, that were electro-polished and conditioned in advance. 250 mL of each whole air sample was injected into a gas chromatography system with mass selective detection/electron capture detection/flame ionization detection (GC-MSD/ECD/FID) for chemical analysis. C_1-C_5 $RONO_2$ as well as their precursors were specified and quantified in this study. In addition, analytical parameters for individual $RONO_2$ are listed in Table S3. More details of sample collection and chemical analysis were described in Text S1 and S2.

2.2 Model application

2.2.1 Observation-based box model (OBM)

A Photochemical Box Model incorporating Master Chemical Mechanism (PBM-MCM) was applied to study the atmospheric oxidative capacity in autumn in Hong Kong. The chemical mechanistic information was taken from a near-explicit mechanism, MCM v3.3 (*http://mcm.leeds.ac.uk/MCM*), including ~6700 species and ~17000 reactions, which considered homogeneous reactions in the boundary layer (Jenkin et al., 1997; Jenkin et al., 2015; Saunders et al., 2003). Observational data (*i.e.* NO, NO_2, SO_2, CO, C_1-C_{10} VOCs and OVOCs, temperature, solar radiation, and relative humidity) were input from 7:00 to 19:00 to constrain the model and reflect the situation in the real atmosphere. Physical processes, including dry deposition, aloft exchange, and atmospheric dilution caused by the variations of the planetary boundary layer height were considered in the model (Lyu et al., 2017a). To achieve localized and optimized simulation results for the study area, model construction was further adjusted, as described in Text S3. This model has been widely applied to simulate photochemistry of secondary pollutants as well as hydroxyl (OH) and hydroperoxyl (HO_2) radicals in Hong Kong (Lyu et al., 2017a; Wang et al., 2017a, 2018). Model performance was repeatedly proven during autumn in Hong Kong in our previous studies with an index of agreement (IOA) ranging from 0.67 to 0.89 for O_3, and 0.45 to 0.97 for $RONO_2$ (Wang et al., 2017a; Liu et al., 2019; Lyu et al., 2017a; Zeng et al., 2018). Since the model did not take into account the vertical/horizontal dispersion, here we only applied this model to simulate in-situ atmospheric oxidative capacity by inputting mixing ratios of observed air pollutants, meteorological parameters and other physical parameters to constrain the box model. Due to the lack of meteorological parameters in 2002, the simulation of ambient oxidative capacity was conducted during 2006-2016.

2.2.2 Positive Matrix Factorization (PMF)

Source apportionment of five C_1-C_4 $RONO_2$ during 2002-2016 (merged as one dataset) was conducted using the PMF model. PMF is a non-negative receptor model developed by the US Environmental Protection Agency (USEPA). Observational datasets are considered as a data matrix *X* of *i* (number of samples) by *j* (number of chemical species) dimensions in the model. Matrix X is decomposed into factor profile *F* and factor contribution *G* (in mass units) to each sample in *p* number of sources, then plus residuals *e*, as shown in Eq. 1:

$$x_{ij} = \sum_{k=1}^{p} g_{ik} f_{ik} + e_{ij} \qquad \text{(Eq. 1)}$$

where x_{ij} represents the mixing ratio of the j^{th} species in the i^{th} sample; g_{ik} represents the contribution of the k^{th} source in i^{th} sample; f_{ik} represents the faction of the k^{th} source in i^{th} sample.

A converged solution with a minimum *Q* value for the *m* number of species in *n* number of samples is given in Eq. 2:

$$Q = \sum_{i=1}^{n} \sum_{j=1}^{m} \left[\frac{x_{ij} - \sum_{k=1}^{p} g_{ik} f_{kj}}{u_{ij}}\right]^2 \qquad \text{(Eq. 2)}$$

where u_{ij} is the uncertainty of the j^{th} species in the i^{th} sample. Two versions of Q are given in the model result. Q(true) includes all data points, while Q(robust) excludes data points with uncertainty-scaled residuals greater than 4. Detailed information and diagnostic parameters of source profiles as well as evaluation on the modelling results were described in Text S4.

3 Results and discussion

3.1 General characteristics

The average mixing ratios of C_1-C_5 $RONO_2$ in autumn during 2002-2016 in Hong Kong are displayed in Figure S3. The mixing ratio of 2-$BuONO_2$ was always the highest ($p < 0.05$) (12.1 ± 3.3 to 54.0 ± 5.6 pptv), followed by *i*-$PrONO_2$ (10.6 ± 2.3 to 30.3 ± 2.6 pptv), $MeONO_2$ (4.8 ± 0.9 to 21.4 ± 2.3 pptv), $EtONO_2$ (3.5 ± 0.7 to 15.0 ± 1.1 pptv), 2-$PeONO_2$ (10.4 ± 1.7 to 15.0 ± 1.8 pptv) and 3-$PeONO_2$ (9.4 ± 1.2 to 10.3 ± 1.6 pptv), while *n*-$PrONO_2$ had the lowest mixing ratio ($p < 0.05$) (1.3 ± 0.4 to 6.2 ± 1.0 pptv). The results were likely caused by the combined effect of increased branching ratio for $RONO_2$ formation, reduced abundances of their precursors and decreased lifetime of $RONO_2$ with increasing carbon number (Arey et al., 2001; Simpson et al., 2006; Zeng et al., 2018). The relative abundances of C_1-C_4 $RONO_2$ remained unchanged during the 15 years, indicating a constant composition of $RONO_2$ in Hong Kong. $MeONO_2$ contributed 10.6 ± 0.2 – 15.8 ± 0.8 % to the total C_1-C_4 $RONO_2$, which was much lower than the proportion (20.6 – 71.0 %) in oceanic air masses, but comparable to that (9.9 – 14.9 %) in continental air masses (Russo et al., 2010; Wang et al., 2013). This suggests a significant influence of continental air flow in autumn in Hong Kong. In most years, the levels of $MeONO_2$ and $EtONO_2$ were comparable, except for the year of 2013, when the mixing ratio of $MeONO_2$ largely surpassed that of $EtONO_2$, possibly implying different allocations of primary emissions in this year. Since $MeONO_2$ is mostly contributed by oceanic emission, wind direction in autumn of each sampling year was further investigated. Higher percentage (80.2%)

of south winds, including southeast and southwest winds, were observed in 2013, indicating more air masses coming from the South China Sea bringing in $MeONO_2$ to Hong Kong compared to other years (66.8-75.5%) (Song et al,, 2018). For the yearly variations, mixing ratios of C_1-C_4 $RONO_2$ seemed to present upward trends until 2013, indicating the enhancement in primary emissions, secondary formation and/or regional transport of $RONO_2$. Significant reductions ($p < 0.05$) for some $RONO_2$, *i.e.* *i*-$PrONO_2$, 2-$BuONO_2$ and 3-$PeONO_2$, were captured in 2016 compared to those in 2013, perhaps related to stringent control of emissions of their precursors and/or weakened atmospheric oxidative capacity that alleviated the levels of $RONO_2$ in this year (Lyu et al., 2017b; Liu et al., 2019; Yao et al., 2019).

3.2 Long-term trends of $RONO_2$

Figure 1 plots the time-dependent variations of C_1-C_4 $RONO_2$ in autumn throughout the period of 2002 – 2016, while C_5 $RONO_2$ was not included due to lack of data points. Long-term trends were estimated based on daily averages using the slope in linear regression method (Kock et al., 2005; Qin et al., 2007; Zhang et al., 2010; Zeng et al., 2020). Error bars (95% CIs) are provided whenever more than one sample was collected per day. The variation rates of some species were not always constant during the whole 2002-2016 period. However, sampling data were distributed equally during the study period and the linear regression method could provide a reliable average trend throughout this period. T-test was conducted and *p* value was calculated to evaluate significance of the changing rates. Pronounced increasing trends ($p < 0.05$) were observed for all $RONO_2$, *i.e.* $MeONO_2$, $EtONO_2$, *i*-$PrONO_2$, *n*-$PrONO_2$ and 2-$BuONO_2$, at average rates of 0.6 ± 0.1 pptv·yr^{-1}, 0.3 ± 0.1 pptv·yr^{-1}, 0.7 ± 0.2 pptv·yr^{-1}, 0.10 ± 0.03 pptv·yr^{-1} and 1.3 ± 0.3 pptv·yr^{-1}, respectively, of which 2-$BuONO_2$ had the highest increasing rate during the study period. Uncertainty brought by different sampling sites is clarified in Text S5 and Table S4. The changing rates of C_1-C_4 $RONO_2$ varied between -0.1 and 0.1 pptv/yr when uncertainties were considered. It is well documented that photochemical secondary formation, biomass burning and oceanic emissions, though they have different allocations on individual $RONO_2$, are main sources of total $RONO_2$, in which secondary formation is the most predominant source in Hong Kong according to previous studies (Lyu et al., 2015; Ling et al., 2016). To further explore the enhancement of $RONO_2$ in Hong Kong, photochemical formation was first studied, based on precursors and/or ambient oxidative capacity during the same time periods as those shown in Figure 1.

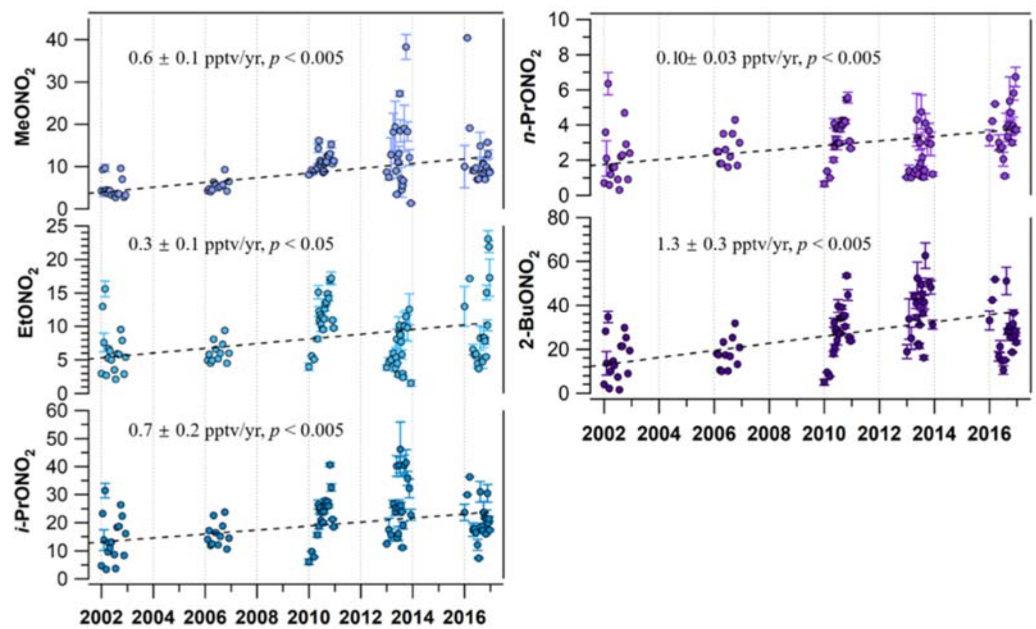

Figure 1. Long-term variations of C_1-C_4 $RONO_2$ in autumn in Hong Kong from 2002 to 2016. Error bars represent 95% CIs of measurement data. The data points are daily averages.

3.3 Long-term variations of $RONO_2$ precursors

The average changing rates of C_1-C_4 parent hydrocarbons (*i.e.* methane, ethane, propane, and *n*-butane) in autumn from 2002 to 2016 with 95% CIs are listed in Table S5. The methane level in Hong Kong slightly decreased in autumn throughout the 15-year study, at a rate of -40.8 ± 3.5 ppbv/yr (part per billion by volume per year, $p < 0.005$), while C_2H_6 and C_4H_{10} remained unchanged ($p > 0.05$) during the study period. Therefore, increments in C_1, C_2 and C_4 $RONO_2$ were not explained by the variations in their parent hydrocarbons. However, a pronounced upward trend ($p < 0.05$) was measured for C_3H_8 from 2002 to 2016, at a rate of 49.8 ± 23.0 pptv/yr (2.6 %/yr), which was slower than the increasing rates of *i*-$PrONO_2$ (3.8 %/yr) and *n*-$PrONO_2$ (3.9 %/yr), suggesting that increased parent hydrocarbons only partially explained the growth in C_3 $RONO_2$ in these years. According to a previous study in Hong Kong (Zeng et al., 2018), other VOCs also contributed to $RONO_2$ formation, particularly for the C_1-C_3 $RONO_2$. For example, $MeONO_2$ production was more sensitive to aromatics, carbonyls and BVOCs, while C_4-C_6 hydrocarbons largely contributed to $EtONO_2$ and *i*/*n*-$PrONO_2$ formation. The average changing trends of these five groups of typical VOC precursors as well as total VOCs (TVOCs) (with 95% CIs) are listed in Table S5. As a group of important precursors of $MeONO_2$, aromatics, *i.e.* propyl benzenes, presented a remarkable decreasing trend at a rate of -240.8 ± 79.0 pptv/yr ($p < 0.005$). No significant changes were found for other groups of VOC precursors. Therefore, variations of VOC precursors, including parent hydrocarbons and other VOCs, could not fully explain the enhancement in ambient $RONO_2$ levels.

Figure 2 shows long-term variations of daily NO_x (*i.e.* NO and NO_2) in autumn during 2002-2016. A continuous dataset of NO_x in autumn from 2002 to 2016 is also plotted in the figure for comparison. NO levels remarkably decreased ($p < 0.05$) in autumn during the VOC sampling years, at a rate of -0.3 ± 0.1 ppbv/yr. A similar downward trend was found in the continuous dataset with a rate of -0.4 ± 0.1 ppbv/yr ($p < 0.005$). In addition, a significant decrease ($p < 0.005$) was discovered in NO_2 levels, at a rate of -0.3 ± 0.1 ppbv/yr during the VOC sampling years and at a similar rate of -0.4 ± 0.07 ppbv/yr for the continuous dataset ($p < 0.005$). The decrease in NO_x was attributable to the previous and on-going air pollution control measures implemented in Hong Kong. For example, the Diesel Commercial Vehicle (DCV) program phases I to III significantly reduced the NO_x level at roadside sites in Hong Kong (Yao et al., 2019; Lyu et al., 2017b). As TC is a suburban site with various anthropogenic activities including transportation, this effect is still obvious. Generally, NO and NO_2 would inhibit the production for most $RONO_2$ while NO_2 facilitates the formation of $MeONO_2$

in Hong Kong (Zeng et al., 2018). Declines in NO_x might stimulate the $RONO_2$ formation to some extent, and this impact would be weakened on $MeONO_2$ formation due to the suppression of decreased NO_2 (Zeng et al., 2018). As this was one of the reasons, other affecting factors were analyzed below.

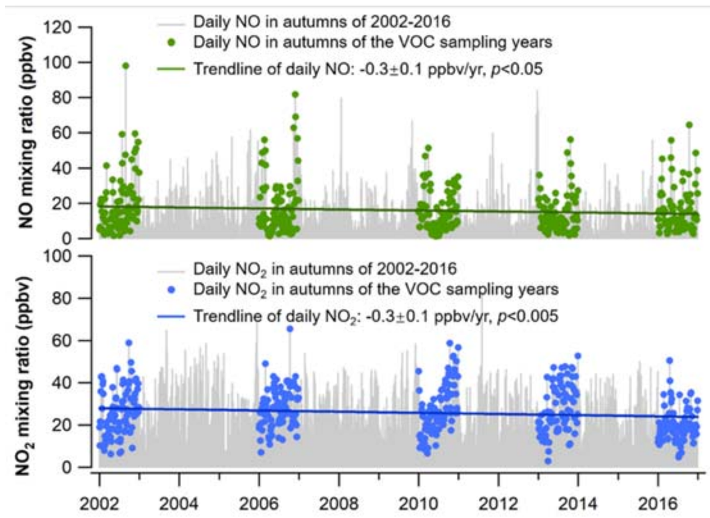

Figure 2. Long-term variations of NO and NO_2 in autumn during 2002-2016 (trendlines of daily NO and NO_2 in this figure are plotted based on daily averages in the autumns of VOC sampling days).

3.4 Atmospheric oxidative capacity in Hong Kong

Concentrations of OH and HO_2 radicals indicate oxidative capacity in the atmosphere, which regulates the formation efficiency of $RONO_2$. Figure S4 displays temporal variations of the simulated OH and HO_2 radicals (by the MCM model) in Hong Kong during 2006-2016. In order to keep consistency of data analysis, we calculated the changing rates based on daily $RONO_2$ averages in 2006, 2010, 2013 and 2016. The continuous OH/HO_2 dataset was also added to the figure for comparison. Levels of OH radicals remarkably increased (p<0.05) in autumn from 2006 to 2016, at a rate of $(1.2 \pm 0.6)\times10^4$ molecules/cm^3/yr. In addition, the trendline of the continuous dataset was similar, with a rate of $(1.0 \pm 0.4)\times10^4$ molecules/cm^3/yr ($p < 0.05$). A significant upward trend ($p < 0.005$) was also discovered in HO_2 levels at $(9.6 \pm 3.1)\times10^5$ molecules/cm^3/yr, while HO_2 stayed invariable in the continuous dataset ($(4.2\pm2.2)\times10^5$

molecules/cm^3/yr, p = 0.05). Trendlines of OH and HO_2 mixing ratios from different starting years to 2016 are shown in Figures S5 and S6, and increasing trends were always found in the study period. Overall, it appears that the elevation in OH and HO_2 radicals increased the oxidative capacity in the atmosphere of Hong Kong, further fueling the secondary $RONO_2$ formation. According to the model simulations, elevation in local formation of $RONO_2$ in Hong Kong could reach 8% with an increase of 20% in OH and HO_2 radicals. The enhancement in atmospheric oxidative capacity in Hong Kong was possibly attributable to the dramatic decrease in NO_x, which consumes OH, HO_2 and RO_2 radicals as well as O_3 in the atmosphere. Yao et al. (2019) reported similar phenomenon that decreased NO_x emissions from LPG vehicles caused O_3 enhancement in Hong Kong. As an important ambient oxidant and indicator of oxidative capacity, O_x presented a significant increasing trend at a rate of 2.0 ± 0.02 ppbv/yr (p<0.05, Figure S7) during the study period.

3.5 Long-term variations of $RONO_2$ sources

3.5.1 Source apportionment of $RONO_2$

Apart from secondary formation, primary sources, *i.e.* oceanic emissions and biomass burning, made non-negligible contributions to ambient $RONO_2$ levels, which are worth investigating. Figure 3 displays the source profiles of ambient VOCs in percentages extracted from the PMF model and six factors were resolved in Hong Kong. Factors were recognized according to loadings of VOC species in the profile.

Factor 1 was associated with large amount of C_2-C_5 alkanes (~20-60%), as well as high percentages of CO (18.5% ± 0.9 %), benzene (19.0 ± 1.1 %), ethene (44.2 ± 1.9 %) and propene (50.0 ± 2.1 %), which are typical tracers in fuel evaporation and vehicle exhaust. Therefore, this factor was determined as vehicle-related emissions. A small fraction of $RONO_2$ (≤ 10%) was found in this factor. Up to now, no research reported the emission of $RONO_2$ in vehicle exhaust or fuel evaporation. The $RONO_2$ in this factor might be caused by the model uncertainty or reflect the residues in the background.

Factor 2 was considered as solvent usage, due to the high allocation of aromatics, such as toluene, *m/p/o*-xylenes and ethylbenzene. Factor 3 was dominated by isoprene, the tracer of biogenic emission. Around 20% of O_3 was also allocated to this factor, possibly due to similar diurnal variations of isoprene and O_3. Both factors 2 and 3 had almost no allocation of $RONO_2$.

Factor 4 was characterized by relatively high percentages of combustion tracers, including CO (30.7 ± 1.9 %), ethane (35.0 ± 1.3 %), ethyne (26.9 ± 1.3 %), benzene (26.9 ± 0.6 %), propene (20.0 ± 1.5 %) and ethene (19.4 ± 0.8 %). A large fraction of biomass burning tracer, CH_3Cl (39.4 ± 0.8 %) was also allocated to this factor. In addition, this factor explained some percentages of ambient $RONO_2$, ranging from 5.5 ± 0.02 % for $MeONO_2$ to 23.9 ± 2.1 % for 2-$BuONO_2$. Therefore, this factor represented biomass burning emissions. Since biomass burning activities have been prohibited in Hong Kong, this factor in Hong Kong was attributable to regional transport from the inland PRD.

Factor 5 was recognized as oceanic emission, in view of the exclusive dominance of DMS (87.3 ± 0.1 %) in this factor. DMS is recognized as the most abundant biological sulfur compound emitted to the atmosphere by the marine phytoplankton (Andreae and Raemdonck, 1983; Dacey and Wakeham, 1986) even though a small fraction of DMS might also be emitted from some industrial processes, like wastewater retreatment (Easter et al., 2005) as well as biomass burning (Friedli et al., 2001). Using DMS as the sole tracer for this factor might overestimate the contribution of oceanic emissions to observed $RONO_2$. $RONO_2$ emitted from this source were mainly C_1-C_3 $RONO_2$, and $MeONO_2$ in this factor reached 25.5 ± 0.1 %.

Factor 6 had high loadings of O_3 (68.4 ± 3.4 %) as well as C_1-C_4 $RONO_2$ (65.0 ± 1.1 % - 72.2 ± 2.1 %). Therefore, this factor represented secondary formation of $RONO_2$. Note that other long-lived species (*i.e.* ethane, ethyne, benzene and CO) were also allocated to this factor, ranging from 31.3 % to 44.5 %, and this factor may contain background residues of secondarily-formed $RONO_2$ as well.

In view of the average source contributions, secondary formation accounted for

67.6 ± 2.8 % (45.5 ± 4.8 pptv) of total observed C_1-C_4 $RONO_2$. The second largest source of $RONO_2$ in Hong Kong during the past 15 years was biomass burning, which occupied 16.6 ± 0.9 % (10.3 ± 1.3 pptv). In addition, 9.8 ± 0.9 % (6.5 ± 1.1 pptv) of observed $RONO_2$ came from oceanic emission. The remaining part (6.0 ± 1.4 %) resolved in other factors was considered as background residues of $RONO_2$ in the atmosphere. Lyu et al. (2015, 2018) reported similar contributions of photochemical formation (69.5 %), oceanic emission (11.3 %) and biomass burning (19.2 %) to C_1-C_4 $RONO_2$ in autumn in southwestern Hong Kong. The results are also consistent with the source contributions in Hong Kong reported by Ling et al. (2016). Surprisingly, the relative contribution of each source (in percentage, as shown in Figure S8) did not vary significantly among different years given the many changes in precursor levels driven by clean air programs, indicating possible influence of regional transport of $RONO_2$ and/or the precursors.

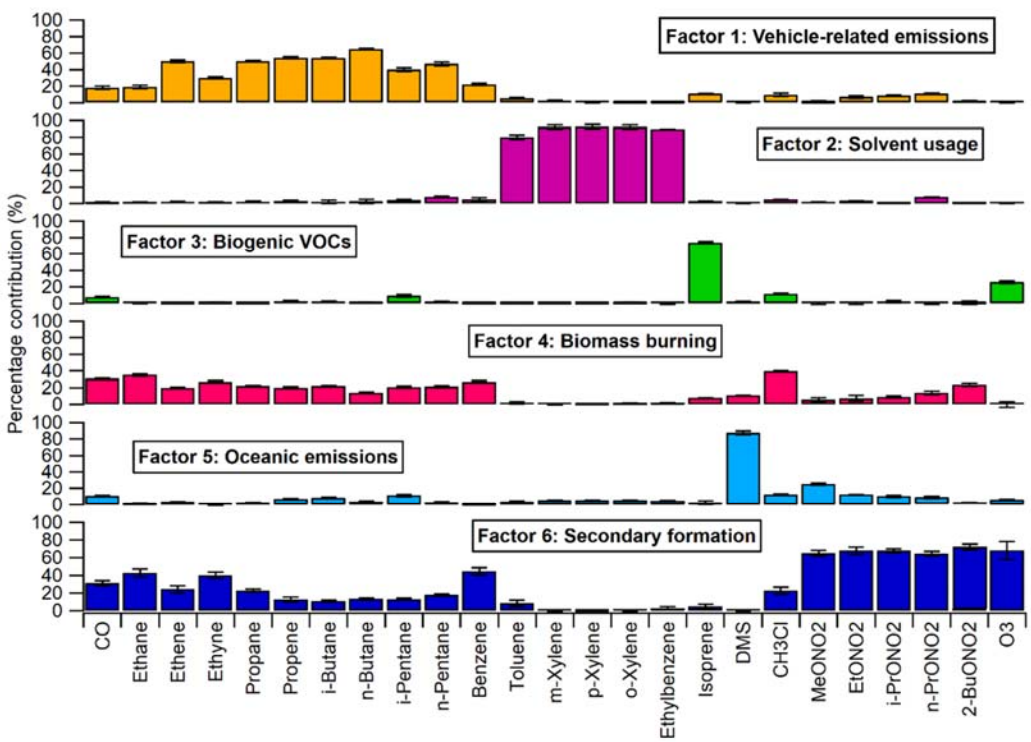

Figure 3. Source profiles of C_1-C_4 $RONO_2$ in Hong Kong (in percentage). Error bars represent 95% confidence intervals, which are estimated by the Bootstrap method.

3.5.2 Temporal variations of $RONO_2$ sources

Mixing ratios of total $RONO_2$ in each source were extracted from the PMF model to investigate temporal variations of $RONO_2$ sources. Figure 4 displays the daily averages of total $RONO_2$ in two primary sources as well as secondary formation during the study period. $RONO_2$ levels in the biomass burning source increased significantly ($p < 0.05$) from 2002 to 2013 at a rate of 0.9 ± 0.2 pptv/yr, then decreased from 2013 to 2016 at 3.0 ± 1.1 pptv/yr, with an average trend of 0.4 ± 0.2 pptv/yr ($p < 0.05$) during 2002-2016. The variation in this source should be related to its variation in inland PRD due to the prohibition of biomass burning activities in Hong Kong. Figure S9 summarizes the satellite fire spots in the PRD region during the study period. Fire spots gradually increased from 2002 to 2013, indicating more and more intensive burning activities in the PRD region, and the situation was relieved in 2016 with fewer fire spots, which was consistent with the results of source variations. Therefore, biomass burning in the PRD region contributed to elevated $RONO_2$ in Hong Kong from 2002 to 2013. In addition, contribution of oceanic emission was relatively stable during the study period, suggesting that the long-term variations of $RONO_2$ in Hong Kong were not influenced by the oceanic emission. Moreover, the contribution of secondary formation to $RONO_2$ enhanced ($p < 0.05$) at a rate of 2.1 ± 0.5 pptv/yr during 2002-2016, which further confirmed the elevation in photochemical formation of $RONO_2$ in Hong Kong, mainly caused by increased atmospheric oxidative capacity, as well as decreased NO_x.

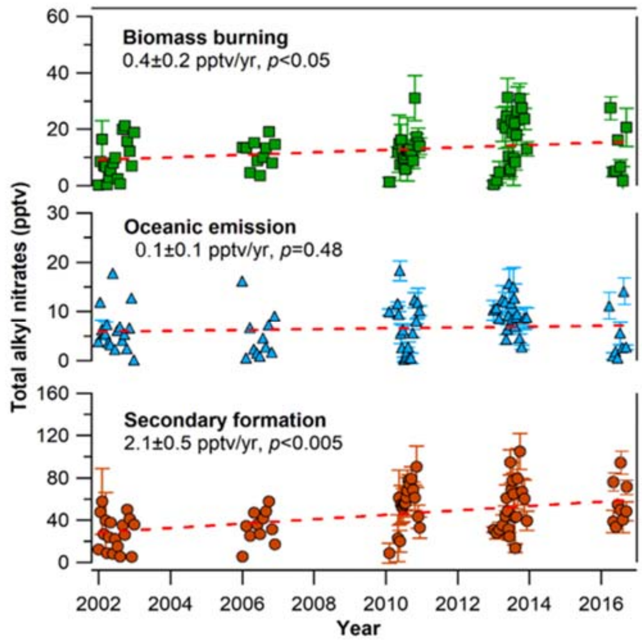

Figure 4. Daily averages of total $RONO_2$ in biomass burning, oceanic emission and secondary formation during 2002-2016 (error bars represent 95% CIs).

3.6 Spatial distributions of $RONO_2$ in Hong Kong and inner PRD region

Figure S10 plots mixing ratios of C_1-C_5 $RONO_2$ in Hong Kong during 2002-2016 versus surface wind fields. Generally, higher wind speeds (1.4±0.1 m/s versus overall average of 1.2±0.1 m/s, $p < 0.05$) were captured in the east directions, mostly from the ocean or along the coastline (Zeng et al., 2018). Looking into $RONO_2$ mixing ratios, the lowest $RONO_2$ levels were observed under the south winds (135°<wind direction (WD)<225°) due to the dilution of clean marine air. Relatively higher values were observed in eastern winds (45°<WD<135°), possibly suggesting the influence of air masses from central Hong Kong and/or eastern inland PRD. Particularly, the highest mixing ratios of $RONO_2$, especially for C_3-C_5 $RONO_2$, were found under northwesterly winds (270°<WD<360°), indicating that regional transport from western inland PRD contributed to the elevation in $RONO_2$ in Hong Kong.

Figure 5 displays the spatial distributions of C_1-C_5 $RONO_2$ in Hong Kong acquired from a grid study in autumn. Higher mixing ratios of $RONO_2$ were observed in the northwest part of Hong Kong, in contrast to much lower levels in the eastern part. This pattern was consistently found for C_1-C_5 $RONO_2$, implying that primary emissions (*i.e.* oceanic emissions and biomass burning activities) might not be the key factor dominating the spatial patterns since C_4 and C_5 $RONO_2$ were predominantly derived from photochemical formation. By further looking into the mixing ratios of parent hydrocarbons and other VOCs, we found that their spatial distributions were different from those of $RONO_2$. For example, relatively low levels of VOC precursors were observed at some sites in the northwest part of Hong Kong. This indicated that part of the $RONO_2$ in northwestern Hong Kong was attributable to regional transport from the inland PRD under the control of northwest winds. Previous studies also reported elevated secondary pollutants, *i.e.* O_3 and $RONO_2$, in Hong Kong when northerly/northeasterly /northwesterly winds dominated in autumn (Guo et al., 2006; Jiang et al., 2010; Ling et al., 2016), and unraveled an increase in the burden of secondary pollutants from inland PRD in Hong Kong (Xue et al., 2014; Wang et al., 2017a). Furthermore, the mixing ratios of C_1-C_5 $RONO_2$ at ten sites over the inner PRD region are plotted in Figure S11, which were obtained by averaging $RONO_2$ levels collected in 2018. Higher concentrations of C_2-C_5 $RONO_2$ were captured in the western PRD region. In view of more abundant VOC precursors as well as higher atmospheric oxidative capacity indicated by higher O_x level (Figure S12) in western PRD, especially in Zhaoqing, Zhongshan, Jiangmen and Zhuhai, higher $RONO_2$ levels in western PRD might be attributed to more intensive photochemical formation. Unlike C_2-C_5 $RONO_2$, spatial distribution of observed $MeONO_2$ did not show an obvious pattern, possibly due to the contribution of oceanic emissions to $MeONO_2$ in the PRD region.

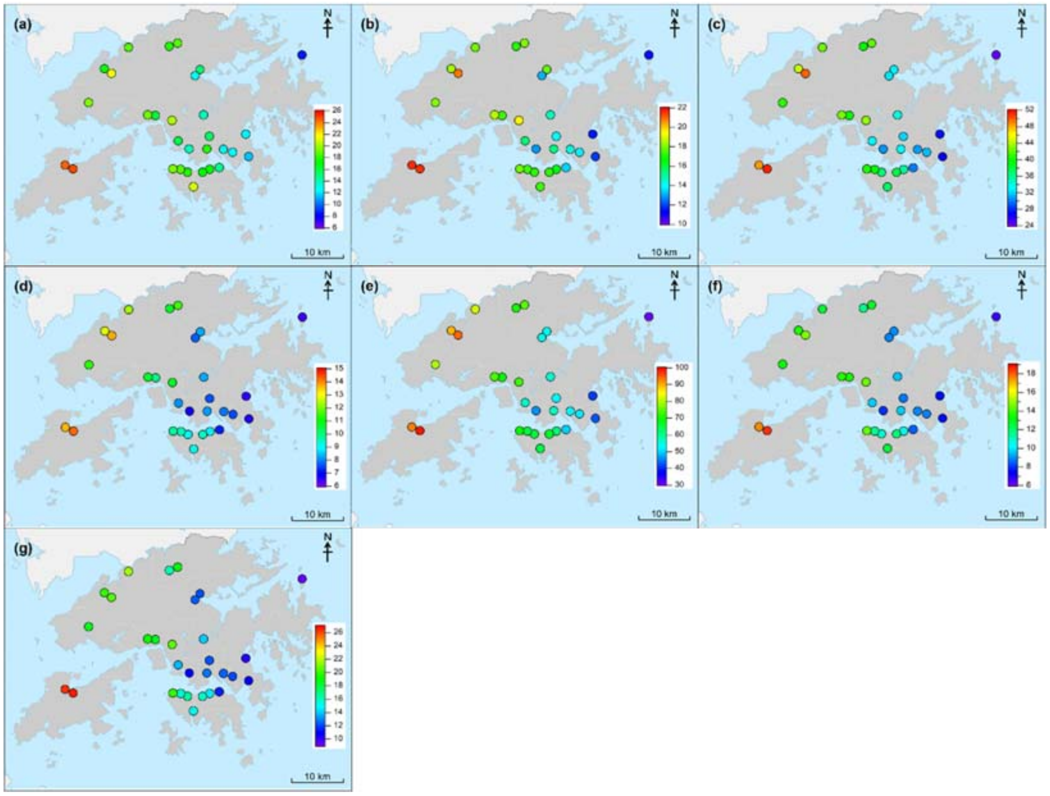

Figure 5. Spatial distributions of mixing ratios of (a) $MeONO_2$, (b) $EtONO_2$, (c) *i*-$PrONO_2$, (d) *n*-$PrONO_2$, (e) 2-$BuONO_2$, (f) 3-$PeONO_2$ and (g) 2-$PeONO_2$ in Hong Kong (units: pptv).

4 Conclusions

Whole air samples were collected in Hong Kong during 2002-2016 to study the long-term variations of ambient C_1-C_5 $RONO_2$, and to investigate the driving factors for their variations in autumn. During the study period, average levels of 2-$BuONO_2$ were always highest, while *n*-$PrONO_2$ had the lowest mixing ratios. Pronounced increasing trends over time ($p < 0.05$) were observed for all $RONO_2$, of which 2-$BuONO_2$ had the highest increasing rate (1.3 ± 0.3 pptv/yr). To determine the causes of elevated $RONO_2$, temporal variations of parent hydrocarbons as well as other VOC precursors were studied. Elevated C_3H_8 might have contributed to the increase in C_3 $RONO_2$, while other VOC precursors remained unchanged or even decreased (CH_4 and aromatics) in these years. In addition, both NO and NO_2 presented dramatic downward trends in autumn from 2002 to 2016, both at a rate of -0.3 ± 0.1 ppbv/yr, which would stimulate the $RONO_2$ formation. This effect was weakened on $MeONO_2$ formation since NO_2 makes a positive contribution to $MeONO_2$ production. Further investigation of atmospheric oxidative capacity showed elevations in both OH and HO_2 radicals during the study period, indicating increased formation efficiency of secondary $RONO_2$ in Hong Kong.

$RONO_2$ sources over the study period were identified and quantified using the PMF model. Six sources of ambient VOCs were specified, including vehicle emissions, solvent usage, biogenic emissions, biomass burning, oceanic emissions and secondary formation, among which secondary formation was the largest contributor to $RONO_2$. The contributions of two primary sources, *i.e.* biomass burning and oceanic emissions, as well as secondary formation of $RONO_2$ in each year were extracted. Elevated secondary formation coincided with the increased formation efficiency of secondary $RONO_2$ in Hong Kong. In addition, elevation in biomass burning was another possible reason for the increased $RONO_2$ in autumn. At last, spatial distributions of $RONO_2$ over the Hong Kong territory revealed that regional transport from inland PRD possibly contributed to the buildup of $RONO_2$ in Hong Kong. Furthermore, more severe $RONO_2$ pollution in the western PRD region was found.

Acknowledgements

This study was supported by the Research Institute for Sustainable Urban Development, Hong Kong Polytechnic University (1-BBW9) and by the Research Grants Council of the Hong Kong Special Administrative Region via Grants PolyU152052/16E and CRF/C5004-15E. This study was partially supported by Hong Kong PolyU internal grants (1-ZVJT and 4-BCF6). We appreciated the use of data and imagery from LANCE FIRMS operated by NASA's Earth Science Data and Information System (ESDIS) with funding provided by NASA Headquarters.

References

Andreae, M. O. & Raemdonck, H. 1983. Dimethyl sulfide in the surface ocean and the marine atmosphere: a global view. Science, 221, 744-747.

Arey, J., Aschimann, S. M., Kwok, E. S. C. & Atkinson, R. 2001. Alkyl Nitrate, Hydroxyalkyl Nitrate, and Hydroxycarbonyl Formation from the NO_x-Air Photooxidations of C_5-C_8 n-Alkanes. Journal of Physical Chemical A, 105, 1020-1027.

Atkinson, R. 1990. Gas-phase tropospheric chemistry of organic compounds: a review. Atmospheric Environment Part A. General Topics, 24 (1), 1-41.

Atkinson, R., Aschmann, S. M., Carter, W. P. L., Winer, A. M. & Pitts, J. N. 1982. Alkyl nitrate formation from the nitrogen oxide (NO_x)-air photooxidations of C_2-C_8 n-alkanes. The Journal of Physical Chemistry, 86, 4563-4569.

Atlas, E., Pollock, W., Greenberg, J., Heidt, L. & Thompson, A. M. 1993. Alkyl nitrates, nonmethane hydrocarbons, and halocarbon gases over the equatorial Pacific Ocean during SAGA 3. Journal of Geophysical Research: Atmospheres, 98, 16933-16947.

Barletta, B., Meinardi, S., Simpson, I. J., Khwaja, H. A., Blake, D. R. & Rowland, F. S. 2002. Mixing ratios of volatile organic compounds (VOCs) in the atmosphere of Karachi, Pakistan. Atmospheric Environment, 36, 3429-3443.

Bertman, S. B., Roberts, J. M., Parrish, D. D., Buhr, M. P., Goldan, P. D., Kuster, W. C., Fehsenfeld, F. C., Montzka, S. A. & Westberg, H. 1995. Evolution of alkyl nitrates with air mass age. Journal of Geophysical Research: Atmospheres, 100, 22805-22813.

Blake, N. J., Blake, D. R., Swanson, A. L., Atlas, E., Flocke, F. & Rowland, F. S. 2003. Latitudinal, vertical, and seasonal variations of C_1-C_4 alkyl nitrates in the troposphere over the Pacific Ocean during PEM-Tropics A and B: Oceanic and continental sources. Journal of Geophysical Research: Atmospheres, 108, D2, 8242, doi:10.1029/2001JD001444.

Carter, W. P. L. & Atkinson, R. 1989. Alkyl nitrate formation from the atmospheric photoxidation of alkanes; a revised estimation method. Journal of Atmospheric Chemistry, 8, 165-173.

Chuck, A. L., Turner, S. M. & Liss, P. S. 2002. Direct Evidence for a Marine Source of C_1 and C_2 Alkyl Nitrates. Science, 297, 1151-1154.

Clemitshaw, K. C., Williams, J., Rattigan, O. V., Shallcross, D. E., Law, K. S. & Cox, R. A. 1997. Gas-phase ultraviolet absorption cross-sections and atmospheric lifetimes of several C_2-C_5 alkyl nitrates. Journal of Photochemistry and Photobiology A: Chemistry, 102, 117-126.

Dacey, J. W. H. & Wakeham, S. G. 1986. Oceanic Dimethylsulfide: Production During Zooplankton Grazing on Phytoplankton. Science, 233, 1314-1316.

Day, D. A., Dillon, M. B., Wooldridge, P. J., Thornton, J. A., ROSEN, R. S., WOOD,

E. C. & COHEN, R. C. 2003. On alkyl nitrates, O_3, and the "missing NO_y". Journal of Geophysical Research: Atmospheres, 108.

Easter, C., Quigley, C., Burrowes, P., Witherspoon, J. & Apgar, D. 2005. Odor and air emissions control using biotechnology for both collection and wastewater treatment systems. Chemical Engineering Journal, 113, 93-104.

Fisher, J. A., Atlas, E. L., Barletta, B., Meinardi, S., Blake, D. R., Thompson, C. R., Ryerson, T. B., Peischl, J., Tzompa-sosa, Z. A. & Murray, L. T. 2018. Methyl, ethyl, and propyl nitrates: global distribution and impacts on reactive nitrogen in remote marine environments. Journal of Geophysical Research: Atmospheres, 123, 12,429-12,451.

Friedli, H. R., Atlas, E., Stroud, V. R., Giovanni, L., Campos, T. & Radke, L. F. 2001. Volatile organic trace gases emitted from North American wildfires. Global Biogeochemical Cycles, 15, 435-452.

Flocke, F., Volz-thomas, A., Buers, H. J., Pätz, W., Garthe, H. J. & Kley, D. 1998. Long-term measurements of alkyl nitrates in southern Germany: 1. General behavior and seasonal and diurnal variation. Journal of Geophysical Research: Atmospheres, 103, 5729-5746.

Guo, H., Wang, T., Blake, D. R., Simpson, I. J., Kwok, Y. H. & Li, Y. S. 2006. Regional and local contributions to ambient non-methane volatile organic compounds at a polluted rural/coastal site in Pearl River Delta, China. Atmospheric Environment, 40, 2345-2359.

Jiang, F., Guo, H., Wang, T. J., Cheng, H. R., Wang, X. M., Simpson, I. J., Ding, A. J., Saunders, S. M., Lam, S. H. M. & Blake, D. R. 2010. An ozone episode in the Pearl River Delta: Field observation and model simulation. Journal of Geophysical Research: Atmospheres, 115.

Jenkin, M. E., Young, J. C. & Rickard, A. R. 2015. The MCM v3.3.1 degradation scheme for isoprene. Atmospheric Chemistry and Physics, 15, 11433-11459.

Jenkin, M. E., Saunders, S. M. & Pilling, M. J. 1997. The tropospheric degradation of volatile organic compounds: a protocol for mechanism development. Atmospheric Environment, 31, 81-104.

Kock, H. H., Bieber, E., Ebinghaus, R., Spain, T. G., Thees, B., 2005. Comparison of long-term trends and seasonal variations of atmospheric mercury concentrations at the two European coastal monitoring stations Mace Head, Ireland, and Zingst, Germany. Atmospheric Environment, 39 (39), 7549-7556.

Ling, Z. H., Guo, H., Simpson, I. J., Saunders, S. M., Lam, S. H. M., Lyu, X. & Blake, D. R. 2016. New insight into the spatiotemporal variability and source apportionments of C_1–C_4 alkyl nitrates in Hong Kong. Atmospheric Chemistry and Physics, 16, 8141-8156.

Liu, X. F., Lyu, X. P., Wang, Y., Jiang, F. & Guo, H. 2019. Intercomparison of O_3

formation and radical chemistry in the past decade at a suburban site in Hong Kong. Atmospheric Chemistry and Physics, 19, 5127-5145.

Lyu, X. P. 2018. Photochemical formation of alkyl nitrates and their impacts on ozone production in Hong Kong. PhD thesis, The Hong Kong Polytechnic University.

Lyu, X. P., Guo, H., Wang, N., Simpson, I. J., Cheng, H. R., Zeng, L. W., Saunders, S. M., Lam, S. H. M., Meinardi, S. & Blake, D. R. 2017a. Modeling C_1–C_4 Alkyl Nitrate Photochemistry and Their Impacts on O_3 Production in Urban and Suburban Environments of Hong Kong. Journal of Geophysical Research: Atmospheres, 122, 10,539-10,556.

Lyu, X. P., Zeng, L. W., Guo, H., Simpson, I. J., Ling, Z. H., Wang, Y., Murray, F., Louie, P. K. K., Saunders, S. M., Lam, S. H. M. & Blake, D. R. 2017b. Evaluation of the effectiveness of air pollution control measures in Hong Kong. Environmental Pollution, 220, 87-94.

Lyu, X. P., Ling, Z. H., Guo, H., Saunders, S. M., Lam, S. H. M., Wang, N., Wang, Y., Liu, M. & Wang, T. 2015. Re-examination of C_1–C_5 alkyl nitrates in Hong Kong using an observation-based model. Atmospheric Environment, 120, 28-37.

Qin, D. 2007. Decline in the concentrations of chlorofluorocarbons (CFC-11, CFC-12 and CFC-113) in an urban area of Beijing, China. Atmospheric Environment, 41 (38), 8424-8430.

Russo, R. S., Zhou, Y., Haase, K. B., Wingenter, O. W., Frinak, E. K., Mao, H., Talbot, R. W., Sive, B. C. 2010. Temporal variability, sources, and sinks of C_1-C_5 alkyl nitrates in coastal New England. Atmospheric Chemistry and Physics, 10(4), 1865-1883.

Saunders, S. M., Jenkin, M. E., Derwent, R. G. & Pilling, M. J. 2003. Protocol for the development of the Master Chemical Mechanism, MCM v3 (Part A): tropospheric degradation of non-aromatic volatile organic compounds. Atmospheric Chemistry and Physics, 3, 161-180.

Simpson, I. J., Wang, T., Guo, H., Kwok, Y. H., Flocke, F., Atlas, E., Meinardi, S., Rowland, F. S. & Blake, D. R. 2006. Long-term atmospheric measurements of C_1–C_5 alkyl nitrates in the Pearl River Delta region of southeast China. Atmospheric Environment, 40, 1619-1632.

Simpson, I. J., Blake, N. J., Blake, D. R., Atlas, E., Flocke, F., Crawford, J. H., Fuelberg, H. E., Kiley, C. M., Meinardi, S. & Rowland, F. S. 2003. Photochemical production and evolution of selected C_2–C_5 alkyl nitrates in tropospheric air influenced by Asian outflow. Journal of Geophysical Research: Atmospheres, 108.

Simpson, I. J., Meinardi, S., Blake, D. R., Blake, N. J., Rowland, F. S., Atlas, E. & Flocke, F. 2002. A biomass burning source of C_1–C_4 alkyl nitrates. Geophysical Research Letters, 29, 21-1-21-4.

Sommariva, R., Trainer, M., De Gouw, J. A., Roberts, J. M., Warneke, C., Atlas, E., Flocke, F., Goldan, P. D., Kuster, W. C., Swanson, A. L. & Fehsenfeld, F. C. 2008. A study of organic nitrates formation in an urban plume using a Master Chemical Mechanism. Atmospheric Environment, 42, 5771-5786.

Song, J. W., Zhang, Y. Y., Huang, Y., Ho, K. F., Yuan, Z. Y., Ling, Z. H., Niu X. J., Gao, Y., Cui, L., Louie, P. K. K., Lee, S. C. & Lai, S. C. 2018. Seasonal variations of C1-C4 alkyl nitrates at a coastal site in Hong Kong: Influence of photochemical formation and oceanic emissions. Chemosphere, 194, 275-284.

Swanson, A. L., Blake, N. J., Atlas, E., Flocke, F., Blake, D. R. & Rowland, F. S. 2003. Seasonal variations of C2–C4 nonmethane hydrocarbons and C_1–C_4 alkyl nitrates at the Summit research station in Greenland. Journal of Geophysical Research: Atmospheres, 108.

Wang, Y., Guo, H., Zou, S., Lyu, X., Ling, Z., Cheng, H. & Zeren, Y. 2018. Surface O3 photochemistry over the South China Sea: Application of a near-explicit chemical mechanism box model. Environmental pollution, 234, 155-166.

Wang, Y., Wang, H., Guo, H., Lyu, X., Cheng, H., Ling, Z., Louie, P. K., Simpson, I. J., Meinardi, S. & Blake, D. R. 2017a. Long-term O_3-precursor relationships in Hong Kong: field observation and model simulation. Atmospheric chemistry and physics, 17, 10919-10935.

Wang, T., Xue, L., Brimblecombe, P., Lam, Y. F., Li, L. & Zhang, L. 2017b. Ozone pollution in China: A review of concentrations, meteorological influences, chemical precursors, and effects. Science of the Total Environment, 575, 1582-1596.

Wang, M., Shao, M., Chen, W., Lu, S., Wang, C., Huang, D., Yuan, B., Zeng, L., Zhao, Y. 2013. Measurements of C_1-C_4 alkyl nitrates and their relationships with carbonyl compounds and O_3 in Chinese cities. Atmospheric Environment, 81, 389-398.

Wang, T., Wei, X. L., Ding, A. J., Poon, C. N., Lam, K. S., Li, Y. S., Chan, L. Y. & Anson, M. 2009. Increasing surface ozone concentrations in the background atmosphere of Southern China, 1994–2007. Atmospheric Chemistry and Physics, 9, 6217-6227.

Wang, T., Guo, H., Blake, D. R., Kwok, Y. H., Simpson, I. J. & Li, Y. S. 2005. Measurements of Trace Gases in the Inflow of South China Sea Background Air and Outflow of Regional Pollution at Tai O, Southern China. Journal of Atmospheric Chemistry, 52, 295-317.

Worton, D. R., Reeves, C. E., Penkett, S. A., Sturges, W. T., Slemr, J., Oram, D. E., Bandy, B. J., Bloss, W. J., Carslaw, N. & Davey J. 2010. Alkyl nitrate photochemistry during the tropospheric organic chemistry experiment. Atmospheric Environment, 44, 773-785.

Xue, L. K., Wang, T., Louie, P. K. K., Luk, C. W. Y., Blake, D. R. & Xu, Z. 2014. Increasing External Effects Negate Local Efforts to Control Ozone Air Pollution: A Case Study of Hong Kong and Implications for Other Chinese Cities. Environmental Science & Technology, 48, 10769-10775.

Yao, D., Lyu, X., Murray, F., Morawska, L., Yu, W., Wang, J. & Guo, H. 2019. Continuous effectiveness of replacing catalytic converters on liquified petroleum gas-fueled vehicles in Hong Kong. Science of The Total Environment, 648, 830-838.

Yin, L., Du, P., Zhang, M., Xu, T. & Song, T. 2019. Estimation of emissions from biomass burning in China (2003-2017) based on MODIS fire radiative energy data. Biogeosciences, 16 (7), 1629-1640.

Zeng, L. W., Dang, J., Guo, H., Lyu, X. P., Simpson, I. J., Meinardi, S., Wang, Y., Zhang, L. Y. & Blake, D. R. 2020. Long-term temporal variations and source changes of halocarbons in the Greater Pearl River Delta region, China. Atmospheric Environment, 234, 117550.

Zeng, L. W., Lyu, X. P., Guo, H., Zou, S. C. & Ling, Z. H. 2018. Photochemical formation of C_1-C_5 alkyl nitrates in suburban Hong Kong and over the South China Sea. Environmental Science & Technology, 52 (10), 5581-5589.

Zhang, F., Zhou, L. X., Yao, B., Vollmer, M. K., Greally, B. R., Simmonds, P. G., Reimann, S., Stordal, F., Maione, M., Xu, L. & Zhang, X. C. 2010. Analysis of 3-year observations of CFC-11, CFC-12 and CFC-113 from a semi-rural site in China. Atmospheric Environment, 44 (35), 4454-4462.